Experimental and numerical investigation of the effect of vertical loading on the lateral behaviour of monopiles in sand

Li, Q.[a,b,1], Gavin, K.G.[a,2], Askarinejad, A.[a,3], Prendergast, L.J.[c,4*]

[a] Faculty of Civil Engineering and Geosciences,
Delft University of Technology,
Building 23,
Stevinweg 1/ PO-box 5048,
2628 CN Delft/ 2600 GA Delft,
The Netherlands

[b] Huadong Engineering (Shenzhen) Corporation Limited,
Shenzhen,
China

[c] Department of Civil Engineering,
Faculty of Engineering,
University of Nottingham,
Nottingham,
NG7 2RD,
United Kingdom

[*]Corresponding author

Email: [1]Q.Li-3@tudelft.nl, [2] k.g.gavin@tudelft.nl, [3]A.Askarinejad@tudelft.nl,
[4]luke.prendergast@nottingham.ac.uk

ABSTRACT

The influence of combined loading on the response of monopiles used to support offshore wind turbines (OWTs) is investigated in this paper. In current practice, resistance of monopiles to vertical and lateral loading is considered separately. As OWT size has increased, the slenderness ratio (pile length, *L*, normalised by diameter, *D*) has decreased, and foundations are tending towards intermediate footings with geometries between those of piles and shallow foundations. Whilst load interaction effects are not significant for slender piles, they are critical for shallow footings. Previous research on pile load interaction has resulted in conflicting findings, potentially arising from variations in boundary conditions and pile slenderness. In this study, monotonic lateral load tests were conducted in a geotechnical centrifuge on vertically loaded monopiles in dense sand. Results indicate that for piles with $L/D = 5$, increasing vertical loading improved pile initial stiffness and lateral capacity. A similar trend was observed for piles with $L/D = 3$, when vertical loading was below ≈ 45% of the pile's ultimate

vertical capacity. For higher vertical loads considered, results tended towards the behaviour observed for shallow footings. Numerical analyses conducted show that changes in mean effective stress are potentially responsible for the observed behaviour.

Keywords: Combined loading, Monopiles, Sand, Centrifuge modelling, *p*-*y* curves

List of notation

A	length of strong box	p_0	lateral soil resistance under zero vertical loading
B	width of strong box	p_V	lateral soil resistance when the applied vertical load is a non-zero value
C_C	curvature coefficient of sand	$P1$	pile (number) 1
C_U	uniformity coefficient of sand	$P2$	pile (number) 2
D	pile outer diameter	$P3$	pile (number) 3
D_{50}	average grain size of sand	R_0	distance from pile pivot point to pile toe
D_r	relative density of sand	R_f	failure ratio
e	load eccentricity	R_{inter}	relative strength of the interface to soil
e_{min}	minimum void ratio of sand	t	pile wall thickness
e_{max}	maximum void ratio of sand	V	vertical load
E	Young's modulus	V_u	pile vertical capacity
E_{50}^{ref}	secant stiffness for CD triaxial test	V_{u_pre}	pile vertical capacity on pre-installed pile
E_{oed}^{ref}	tangent oedometer stiffness	y	lateral displacement
E_{ur}^{ref}	unloading reloading stiffness	z	depth in the soil from mudline
g	gravitational acceleration rate	α	pile rotation angle
Gs	specific gravity of sand	ϑ	normalized pile lateral capacity
H_u	pile lateral capacity	ρ	pile curvature
H	lateral load	φ	friction angle of sand in numerical simulation
$H_{u,0}$	pile lateral capacity under zero vertical loading	φ_{cr}	critical friction angle of sand in physical modelling
$H_{u,V}$	pile lateral capacity when the applied vertical load is a non-zero value	ν	Poisson's ratio
I	moment of inertia	ν_{ur}	Poisson's ratio for unloading-reloading
k_{ini}	initial stiffness	γ'	effective unit weight of sand
L	pile embedded length	ψ	angle of dilation
L_T	total length of model monopile	χ	improvement in soil resistance
m	power of stress-level dependency of stiffness	ζ	improvement in mean effective stress
M	bending moment	$\sigma_{m,0}$	mean effective stress under zero vertical loading
p	lateral soil resistance	$\sigma_{m,V}$	mean effective stress when the applied vertical load is a non-zero value
p^{ref}	reference stress for stiffness		

1 Introduction

The development of OWTs has experienced rapid growth in recent years and is considered the most mature technology to facilitate the energy transition (Li et al., 2018). Monopiles remain the most commonly used foundation to support OWTs accounting for 87% of all installations to 2019 (WindEurope, 2018; Fan et al., 2019). Monopiles comprise single open-ended steel tubes driven into the seabed. Typical pile sizes used to support early OWTs had diameters, D, in the range 4 to 6 m and embedded lengths, L, in the range 20 to 30 m, with L/D between 5 and 6 (Doherty and Gavin, 2012). As turbines grow to 10 MW, the pile diameter required to limit pile mudline rotation is increasing to between 8 m and 10 m (Byrne et al., 2015). The combination of relatively low turbine weight and large pile diameter means embedded lengths of monopiles has not increased significantly and L/D ratios have reduced towards values in the range 2 to 3. Although referred to as monopiles, these are more correctly termed intermediate foundations, which are classified in ISO 1990-1-4 as having L/D in the range 1 to 10.

Several authors have studied combined loading for shallow and skirted foundations. Interaction effects can occur such that the lateral load, H, and moment, M, capacity of footings depend on the current vertical load level, V (Nova and Montrasio, 1991, Butterfield and Gottardi, 1994, Bransby and Randolph, 1998). Whilst a number of studies have considered load-interaction effects on piles, very few have investigated monopile behaviour. Karasev et al. (1977) conducted full-scale combined load tests on cast-in-place concrete piles (D = 600 mm, L = 3 m and L/D = 5) in sandy loam. Test results indicate that vertical loads have a beneficial effect on the lateral load response of piles (the lateral displacement of piles was observed to decrease considerably with increasing vertical load). Jain et al. (1987) performed laboratory combined load tests on fully and partially embedded long flexible open-ended piles (D = 32 mm, L = 1000 mm and L/D = 31.25) installed in sand with a relative density (D_r) of 78%. They reported that the application of vertical loads increased lateral displacements of the pile. Lee (2008) performed laboratory pile tests to assess the influence of vertical loading on the lateral response of piles in sand. Installation effects were considered by testing driven and non-displacement piles. Tests were performed in sand where D_r varied between 38% and 91%. The piles had D = 30 mm, L = 1100 mm and L/D of 37. Similar to the findings of Jain et al. (1987), the authors observed that lateral displacements of the pile head increased with increasing vertical load. Mu et al. (2018) performed combined load tests in a geotechnical centrifuge, where the monopile had D = 6 m, L = 50 m and L/D = 8.3 (at prototype scale) installed in fine, dry sand with relative density of 79%. Strain gauges were installed on the pile to study the influence of vertical loading on the bending moment and lateral soil resistance-displacement (p-y) curves. It was found that the presence of vertical loading decreased the lateral displacement of the monopile. Lu and Zhang (2018) reported centrifuge tests where combined loads were applied to a pile with D = 1 m, L = 16.5 m and L/D = 16.5. They also found that lateral displacements measured at a given applied lateral load decreased as the vertical load increased.

In summary, Karasev et al. (1977), Mu et al. (2018) and Lu and Zhang (2018) suggest that the presence of vertical loading improves pile performance (reduces lateral displacements). In contrast, Jain et al. (1987) and Lee (2008) report the opposite effect. The nature of the response appears to be a trade-off between the p-delta influence, whereby vertical loads applied to laterally displaced piles induce additional moments exacerbating deflections; and vertical loads increasing the stiffness at the pile-soil interface subsequently reducing lateral deflections. Additional reasons for this discrepancy might be related to variations in the pile top fixity applied in the experiments and the range of L/D considered. There is further uncertainty surrounding how the sequence of load application, soil density and soil type influence the responses. Notwithstanding the contradictory results, there is a dearth of data, which consider pile performance under a range of vertical loads, L/D ratios, and installation methods under controlled loading and soil conditions. Interested readers are referred to Li et al. (2020c) for a comprehensive review of the topic.

In this paper, the effect of vertical loading on the lateral response of monopiles used to support OWTs is examined using centrifuge testing. The effect of pile slenderness ratios typically adopted for OWTs on the lateral load capacity and *p-y* curves for monopiles installed in dense sand is studied. In order to assess the impact of installation stress on the pile response, a series of tests are compared where piles are both installed in-flight and pre-installed.

2 Experimental methodology

2.1 Facility and model monopile instrumentation

The experiments in this paper were undertaken using the beam centrifuge at Delft University of Technology (Allersma, 1994; Li et al., 2020d; Zhang and Askarinejad, 2019b). A brief summary of the testing is provided herein. Three aluminium tubular model piles with outer diameter, D = 18 mm, and wall thickness, t = 1 mm were fabricated, termed herein as *P1*, *P2*, and *P3*. To create the scaled models, similitude between the flexural stiffness (EI) of the prototype and model piles is conserved. The properties of these piles at both model and prototype scales are provided in Table 1. *P1* was instrumented with ten strain gauges while *P2* and *P3* were not instrumented. The gauges and cables on *P1* are protected by a 0.5 mm thick layer of epoxy coating, which increases the pile wall thickness and roughness. This may result in a larger pile lateral resistance in the experiments conducted. A photograph of the instrumented pile (*P1*) and one un-instrumented pile (*P3*) is shown in Figure 1.

Table 1. Model and corresponding prototype pile dimensions and properties of test piles

Pile ID	Strain gauge	Model					Prototype*		
		L_T (mm)	E (GPa)	D (mm)	t (mm)	L/D (-)	E (GPa)	D (m)	L/D (-)
P1	10 pairs	240	70	18	1	5	210	1.8	5
P2	None	240	70	18	1	5	210	1.8	5
P3	None	204	70	18	1	3	210	1.8	3

*Assuming prototype pile is fabricated from steel and *g*-level = 100 (*g*, gravitational acceleration).

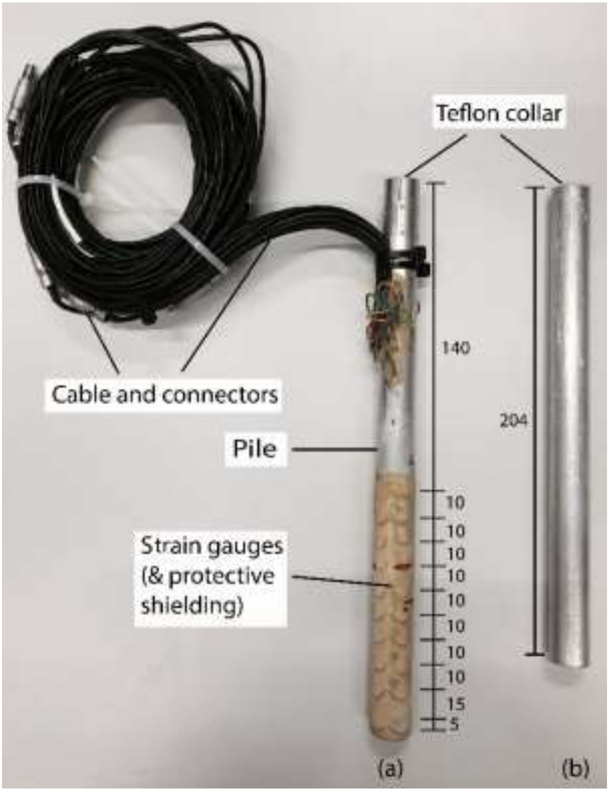

Figure 1 Photograph of model monopiles: (a) *P1* and (b) *P3* (unit: mm)

The piles simulate a 1.8 m diameter steel pipe pile with t = 30 mm at prototype scale (tested at 100*g*), and were installed by jacking to L/D ratios of 3 or 5. It should be noted that the prototype dimensions are smaller than those typically observed for offshore piles, this is a result of the limitations in the permissible pile geometry to avoid boundary effects (elaborated below) and the maximum acceleration field that can be implemented in the centrifuge. However, the slenderness ratio is within the expected range. The terminology used to describe the pile response is summarized in Figure 2; L refers to pile embedded length, e is loading eccentricity, R_0 is distance from the pile pivot point to the pile toe, H is applied lateral load, y is pile lateral displacement at any height along the pile, and α is pile rotation angle. The loading eccentricity, e, was maintained constant in all tests at $8D$.

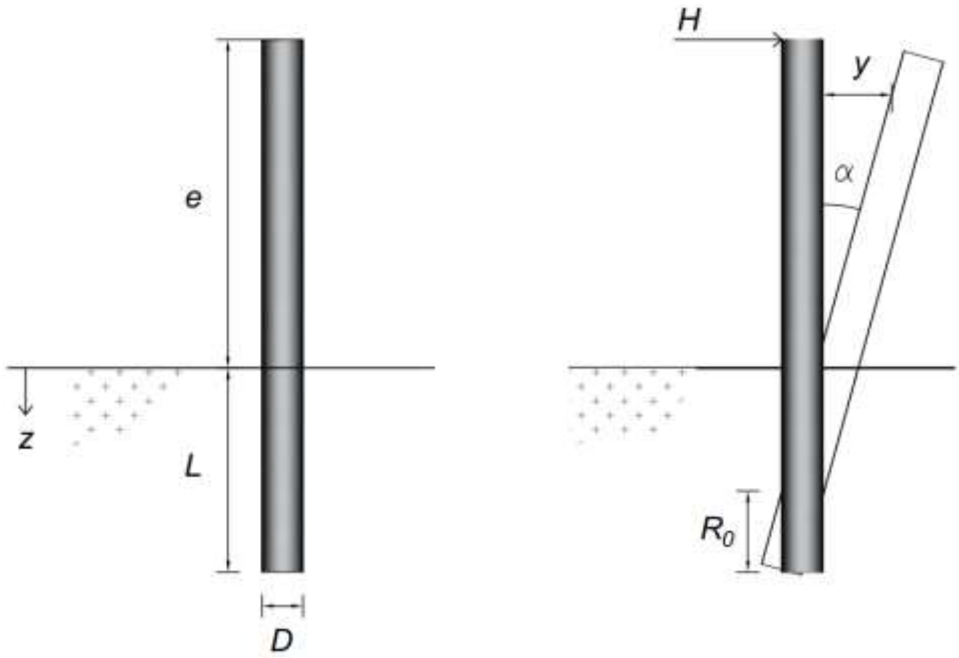

Figure 2 Sketch of pile

2.2 Soil preparation and characterisation

Piles were installed in dense dry Geba sand with D_r = 80% formed using an air pluviation technique. The geotechnical parameters of Geba sand are provided in Table 2 (Maghsoudloo et al., 2018). The critical state friction angle (φ_{cr}) is 35°, which is obtained from drained triaxial tests performed on sand specimens with D_r = 80% up to the axial strain at least 20% (~17.7% shear strain). The silica sand is quite sub-angular. The ratio of outer pile diameter to average grain size of the sand (D/D_{50}) is approximately 164, which is sufficient to avoid particle size effects (Nunez et al., 1988; Dyson and Randolph, 2001; Verdure et al., 2003; Garnier et al., 2007; Klinkvort and Hededal, 2010; Zhang and Askarinejad, 2019a). The ratio of wall thickness to mean particle size t/D_{50} is 9.1, which is very close to the suggested limiting value of 10 (De Nicola, 1996; De Nicola and Randolph, 1997) to avoid particle-size effects from influencing the interaction between the pile annulus and the soil. The plan dimensions of the sand sample are 410 mm by 150 mm, with a sample depth of 155 mm. The ratio of the smallest size of the box to the pile diameter is 8.3, which is larger than the limiting value of 4 as suggested by Prakasha et al. (2005). For the largest pile embedment ratio (L/D = 5), the distance from the pile tip to the bottom of the strong box is $3.6D$, which is larger than the minimum value of $3D$

required to avoid boundary effects (Prakasha et al., 2005). It should be noted that for centrifuge testing there is a trade-off between how large the distances to the boundaries can be while still using an appropriately large pile model to obtain sensible results. It is acknowledged that the distances to the boundaries, though larger than suggested in Prakasha et al. (2005), are still quite minimal in the present work. A brief numerical study was undertaken to ascertain if the boundaries of the present model adversely influenced the findings, and the results suggested that their influence is minimal – more information is provided in section 4 of the paper.

Table 2. Geotechnical properties of Geba sand (De Jager et al., 2017, Maghsoudloo et al., 2018)

e_{min}	e_{max}	Gs	D_{50} (mm)	C_C	C_U	φ_{cr}
0.64	1.07	2.67	0.11	1.24	1.55	35º

2.3 Pile installation and test procedure

Piles were installed using a displacement-controlled actuator at a rate of 0.05 mm/s. The instrumented pile *P1* was jacked to its final penetration depth 5D at 1g (in order to avoid potential damage to the strain gauges and connecting cable by the high stresses when installing at 100g). The remaining uninstrumented piles were jacked to an initial depth of 2D at 1g to maintain vertical stability at elevated g-levels, see Figure 3(a). Following this initial jacking, the centrifuge was spun-up to 100g and the piles were jacked to their final embedment depth 5D (*P2*) and 3D (*P3*), see Figure 3(b).

Installing piles by jacking in place at 1g or in-flight at 100g deviates from what would typically occur offshore, whereby piles are typically impact-driven to penetration, which results in potential differences in mobilised residual base stresses that might be developed in the real case. It was not possible to install the piles by driving at 100g as this would require stopping the centrifuge to adjust the loading rig for the subsequent lateral load application, which would add uncertainty surrounding the influence of the sample stress history on the results obtained (Li et al., 2020). It is noteworthy that the mobilisation of residual stresses may lead to additional base moments on the piles when subjected to lateral loading (Murphy et al., 2018), which are not encountered in the present case. Dyson and Randolph (2001) and Fan et al. (2019) have shown that pile installation method (in-flight driven and jacking) exhibits a reasonable impact on the pile lateral resistance (around 10-20%). The results in this paper consider piles with the same installation approach so the global differences between driven and jacked are less important, but the results should still be considered in this regard.

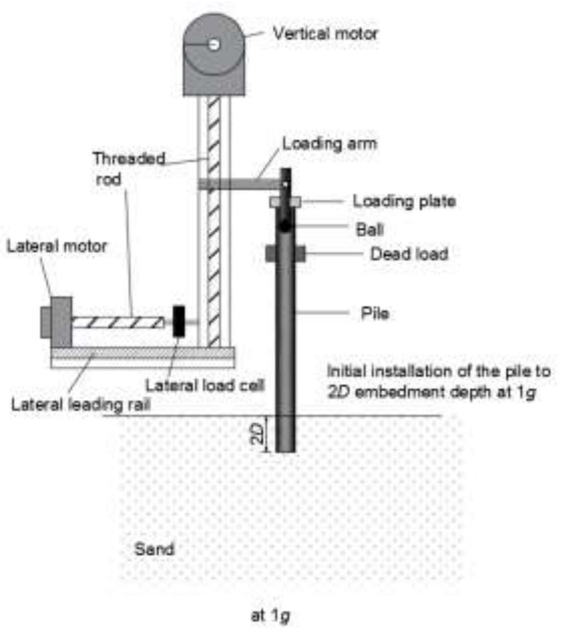

(a)

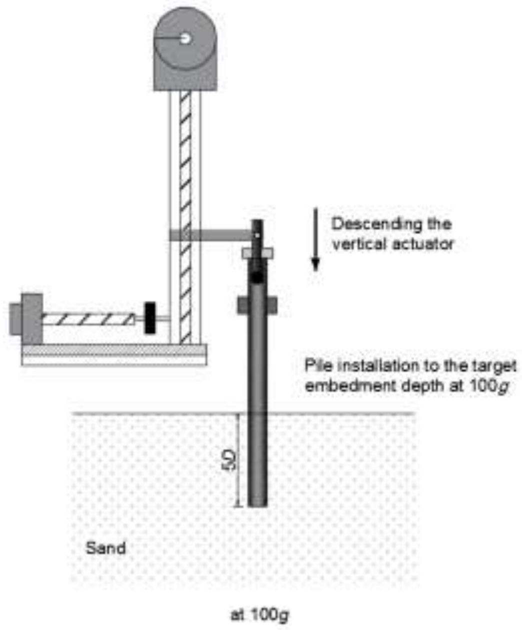

(b)

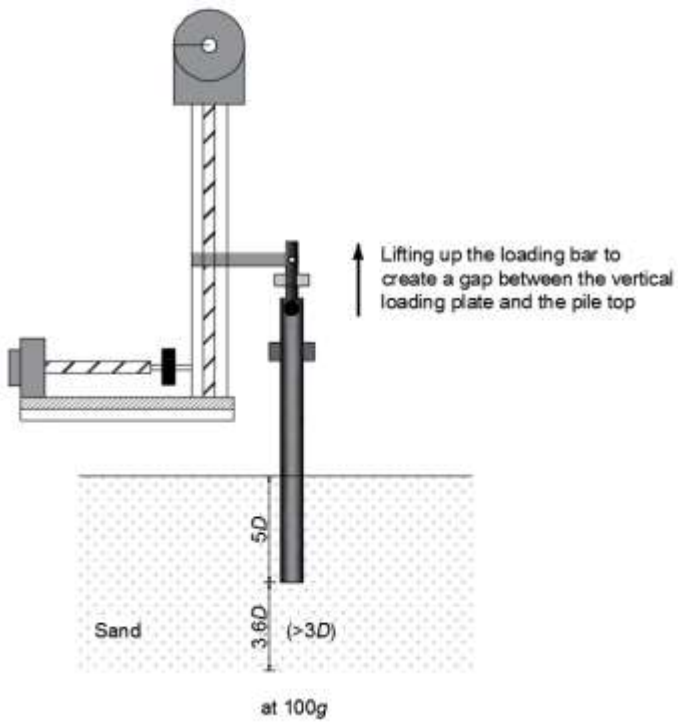

(c)

Figure 3 Schematic showing in-flight pile installation procedures: (a) Initial installation of the pile to 2D embedment depth at 1g; (b) Pile in-flight installation (5D embedment depth shown as an example); (c) Raising of actuator to accommodate subsequent lateral load test

A friction-reducing ball connection (Li et al., 2020b) was used to transfer lateral loads produced by the actuator to the pile head, see Figure 4. The ball was placed vertically into the open-end of the pile head, where it rested in contact with the internal wall of the pile. Between the pile inner surface and the ball, a Teflon collar was used to minimize interface friction.

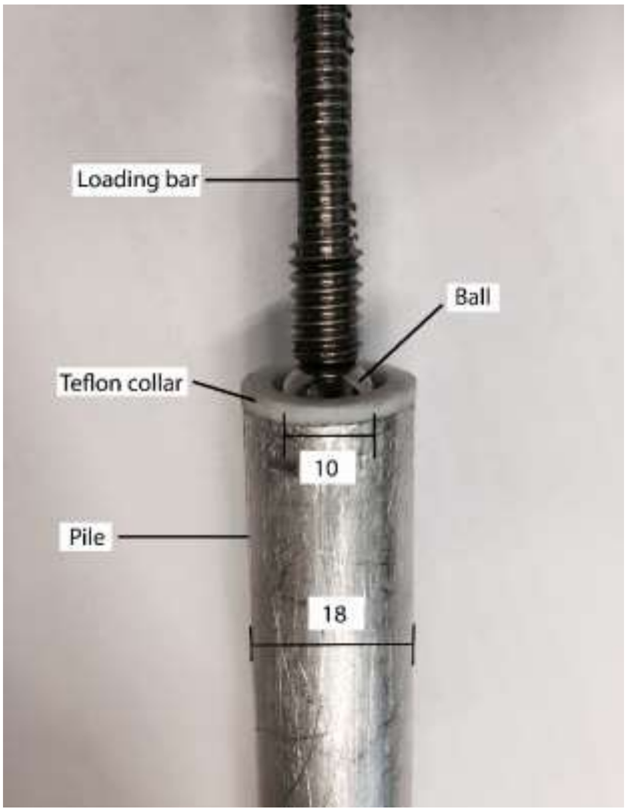

Figure 4 Ball connection for reducing pile-head constraint (dimensions in mm)

In the combined loading tests, the vertical load (V) was fixed on the pile using dead weights prior to pile installation. During the combined loading tests, the lateral load (H) for the pile installed at 1g was monitored at the pile head by parallel beam load cells (HTC-SENSORS TAL220) with a measuring range of ±100 N and sensitivity 0.05%, see Figure 5.

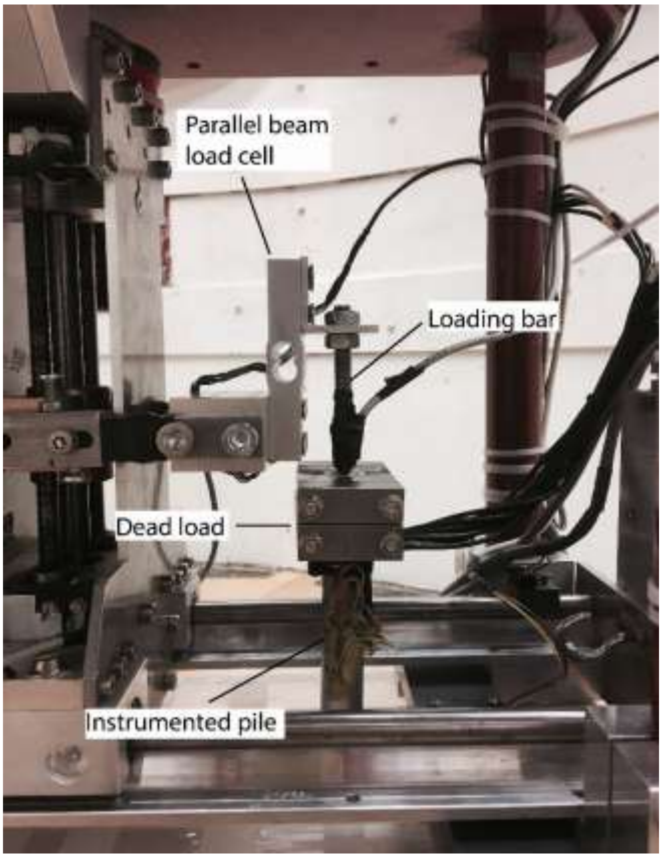

Figure 5 Picture of arrangement of testing components on the instrumented pile (pile *P1*)

In order to perform lateral tests following in-flight installation without stopping the centrifuge, a load cell with measurement capacity of 200 N (SIMBATOUCH SBT650) was placed between the lateral motor and vertical loading tower, see Figure 3(a). The parallel beam load cell cannot be used in this test program, due to the potential high bending moment caused by pile vertical installation. The vertical and lateral displacements of the pile at the loading position (pile head) can be monitored by vertical and lateral motor encoders, which have an accuracy of approximately 3×10^{-5} mm. Any compliance within the system is assumed minimal as the movements of the pile are expected to be significantly larger than these.

The experimental programme comprises 14 centrifuge tests, summarised in Table 3. Tests are described using pile number, acceleration level during installation, and test type/nature. For example, P1-1g-L1 refers to the 1st lateral load test performed on pile *P1*, installed at 1g. Each test was conducted twice to ensure repeatability. The initial stiffness during each test, k_{ini}, is also documented in Table 3.

Table 3. Summary of pile test programme

Test number	Pile L/D	Test nature	Vertical load	k_{ini} (MN/m)
P2/P3-100*g*-V	2*	Obtain vertical capacity (V_u)	0 to V_u	-
P1-1g-V	5**			
P1-1*g*-L1	5	Assess influence of vertical loading on lateral capacity	0	9.2
P1-1*g*-L2	5		$0.15V_u$	10.2
P1-1*g*-L3	5		$0.225V_u$	11.5
P1-1*g*-L4	5		$0.3V_u$	12.2
P2-100*g*-L1	5	Assess influence of vertical loading on lateral capacity	0	11.5
P2-100*g*-L2	5		$0.225V_u$	13.1
P2-100*g*-L3	5		$0.45V_u$	15.3
P2-100*g*-L4	5		$0.675V_u$	16.7
P2-100*g*-L5	5		$0.9V_u$	20.4
P3-100*g*-L6	3		0	1.8
P3-100*g*-L7	3		$0.27V_u$	3.6
P3-100*g*-L8	3		$0.55V_u$	4.9
P3-100*g*-L9	3		$0.82V_u$	7.6

*Pile has 2*D* initial embedment before the vertical load test begins
**Pile has 5*D* initial embedment before the vertical load test begins

3 Experimental results

3.1 Vertical load-displacement response

The vertical load capacity V_u of each pile is firstly determined by means of load testing, corresponding to the first two cases in Table 3. For piles installed in flight (*P2* and *P3*), V_u was defined as the vertical load (jacking force) required to achieve the target penetration. Figure 6 shows the results of the vertical load vs displacement response for piles *P1-P3*, and it can be seen that the results from repeat tests are consistent (the repeat test for *P1* is also consistent but is omitted from the plot for clarity). The vertical capacity for *P3*, with L/D = 3, is 12 MN; and *P2*, with L/D = 5, is 20 MN. It should be noted that for piles *P2* and *P3*, the vertical load vs displacement response exhibits an increased slope for penetrations exceeding 6*D*. This possibly occurs as a result of boundary effects whereby the pile tip approaches the location of the bottom of the box. The effect of installation method is evident from the initial stiffness of *P1*. For consistency, V_u of *P1* is assumed to be equal to *P2* in subsequent analyses.

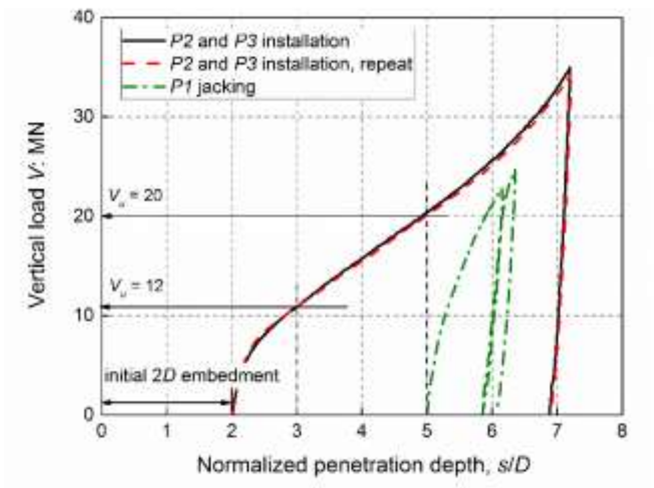

Figure 6 Determination of the vertical load capacity of the tested piles

3.2 Lateral load-displacement response under vertical loading

In this section, lateral load-displacement behaviour of each pile for each of the cases detailed in Table 3 is reported.

The effect of installation stress is considered in Figure 7, where lateral load-displacement response curves for the piles with L/D = 5 are shown. The pile installed in-flight (P2-100*g*-L1) exhibits both larger initial stiffness (k_{ini}) and lateral resistance than that of the pile pre-installed at 1*g* (P1-1*g*-L1). This suggests retention of high mean effective stresses caused by the installation process affects the lateral load-displacement response even at very large lateral displacements. When the pile was installed in-flight, the amount of surface heave is reduced which leads to greater densification of the sand over the upper few diameters (Dyson and Randolph, 2001). The inner filling ratio (plug length of the sand divided by the pile embedment length) was $\approx$ 55%. In the pre-installed case, fully coring behaviour was observed (no plugging). The same trend is evident in Figure 7 for combined load tests where the vertical load was fixed at $0.225V_u$. It is suggested that results might be valid for smaller diameter piles with intermediate embedment, as well as large-diameter monopiles.

The ultimate lateral load capacity H_u is defined as the resistance developed when the pile head displacement at the mudline level reaches $0.1D$ (Lee, 2008). Although both piles in Figure 7 are seen to develop lateral resistance that increase with displacement, H_u is defined as 0.64 MN and 0.93 MN for *P1* and *P2*, respectively.

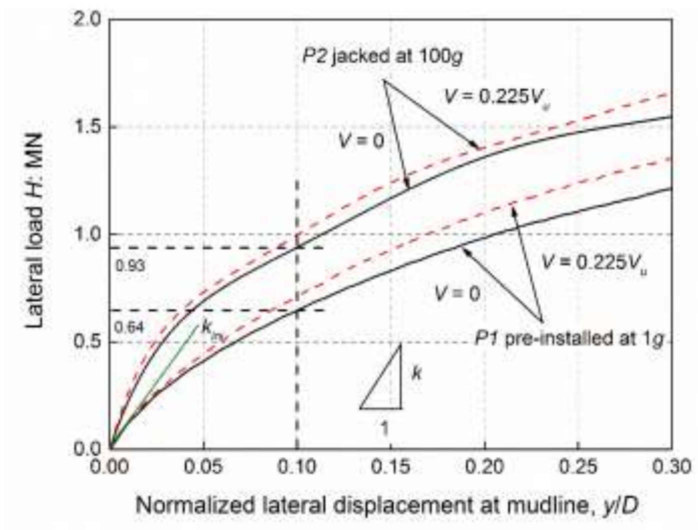

Figure 7 Influence of pile installation stress level on the lateral load-displacement relationship (L/D = 5)

The influence of vertical loading on the lateral load-displacement response for the piles installed to L/D = 5 are compared in Figure 8. It is apparent that an increase in vertical load resulted in an increase in both initial stiffness and lateral capacity of each pile. This trend is broadly similar for piles pre-installed at 1*g* and jacked at 100*g* within the mudline lateral pile displacement range 0 to 0.1*D*.

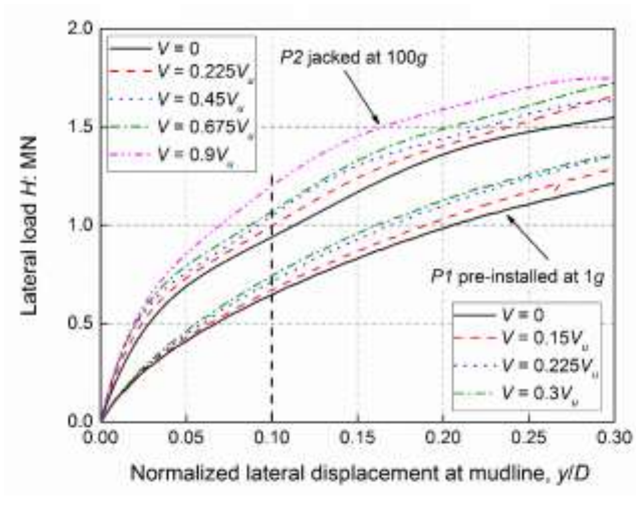

Figure 8 Influence of vertical loading on the lateral load-displacement relationship: piles pre-installed at 1*g* and jacked at 100*g* (L/D = 5)

The likely mechanism controlling the increase in initial stiffness and the lateral capacity in the presence of vertical loading is the increased mean effective stress level in the sand caused by the pre-application of vertical loads. This causes an increase in sand stiffness and strength thereby increasing lateral resistance (Karthigeyan et al., 2007; Lu and Zhang, 2018), which is investigated numerically in section

4. The experimental results presented in Figure 8 are consistent with the centrifuge study of Mu et al. (2018) and Lu and Zhang (2018).

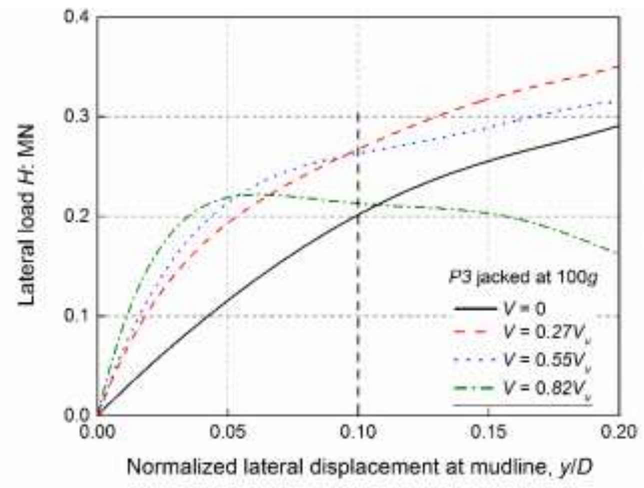

Figure 9 Influence of vertical loading on the lateral load-displacement relationship for pile jacked at 100*g* (L/D = 3)

The influence of vertical loading on the lateral load-displacement response for piles installed to L/D = 3 is shown in Figure 9 (see Table 3). The data show that the initial stiffness increased with the application of vertical loading. Pile lateral resistance also increased up to a lateral mudline displacement of approximately 0.05D. For the tests with applied vertical loads of 0, 0.27V_u and 0.55V_u, lateral resistance continued to increase with increasing lateral displacement. However, the rate of increase for the pile with a vertical load of 0.27V_u is higher than for the pile with 0.55V_u, such that at mudline displacement y/D = 0.1, the lateral capacity measured in both tests was approximately equal. In the test where the applied vertical load is 0.82V_u, the resistance reduces for mudline displacements larger than 0.05D, and the H_u value at mudline displacement y/D = 0.1 is only slightly higher than the pile with no vertical load. From the data it is clear that L/D and V/V_u have an influence on the load-interaction response of monopiles.

The influence of vertical loading on the pile lateral capacity (H_u) can be expressed by the following equation (Karthigeyan et al., 2007; Mu et al., 2018):

$$\vartheta = H_{u,V}/H_{u,0} \qquad \text{Equation 1}$$

where ϑ is normalized pile lateral capacity; $H_{u,V}$ is pile lateral capacity when applied vertical load is non-zero; and $H_{u,0}$ is pile lateral capacity under lateral loading only (V = 0). The data in Figure 9 make it clear that ϑ is very sensitive to the mudline displacement y/D value at which the pile lateral capacity is defined.

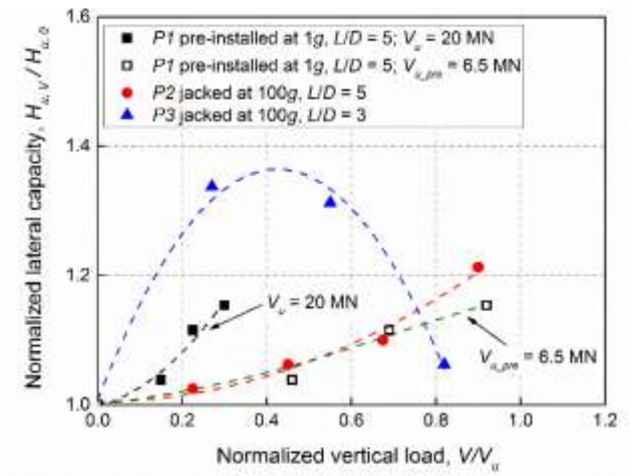

Figure 10 Influence of vertical loading on the lateral capacity of the model piles

A summary of the ϑ values from all tests is shown in Figure 10, which reveals:

1. For the range of parameters considered, ϑ is always greater than unity, meaning the application of vertical loading reduces corresponding lateral displacements.
2. For piles with L/D = 3, lateral capacity increases initially as vertical load increases. The normalized pile lateral capacity reaches a peak value when the vertical load is between $0.4V_u$ and $0.5V_u$. For higher loads the beneficial effect of vertical loading reduces. A parabolic failure locus similar in shape to those reported for shallow foundations by Nova and Montrasio (1991) appears to match the pile response well. However, for shallow foundations discussed in Nova and Montrasio (1991), the lateral capacity is zero when the applied vertical load is zero (assuming the foundation weight can be ignored and there is no embedment) ($V = 0$, $H = 0$). When applied vertical loads increase, the bearing stress between the foundation and sub-soil increases, which increases the lateral capacity through mobilised friction ($0 < V < V_u$, $0 < H$). However, when applied vertical loads surpass a certain threshold, post-failure conditions occur and lateral capacity is reduced to zero ($V = V_u$, $H = 0$). This fundamentally differs from pile behaviour whereby lateral capacity largely depends on pile rigidity, therefore even when applied vertical loads are zero, pile lateral capacity is a non-zero value ($V = 0$, $0 < H$).
3. For piles with L/D of 5, pile lateral capacity increases non-linearly with increasing vertical loads, and the benefit increases as vertical load level increases. At a given V/V_u the beneficial effect is smaller than that seen on the pile with L/D = 3 for V/V_u below 0.8.
4. Comparing data for *P1* and *P2* with L/D = 5, the results are very sensitive to the V_u chosen for the normalisation. Whilst V_u was measured directly for *P2* and *P3* as the jacking force required for installation, see Figure 6, *P1* was jacked at 1g and thus the V_u that should be adopted in the

normalisation is not straight-forward to define. A vertical load test performed in-flight from an initial embedment depth of 5D on this pile is shown in Figure 11. It is clear that a very large displacement of 0.9D was required to mobilise V_u of 20 MN adopted for consistency with *P2* (thus the pile embedment length is 5.9D). An alternative definition of V_u that might be more in keeping with the stress state effective at the time of the lateral load test is to define V_u as the point at which pile stiffness decreases significantly in the vertical load test. From Figure 11 an alternative definition of V_{u_pre} for *P1* is 6.5 MN. Replotting the data in Figure 10 with this lower V_u value shows comparable behaviour with *P2*.

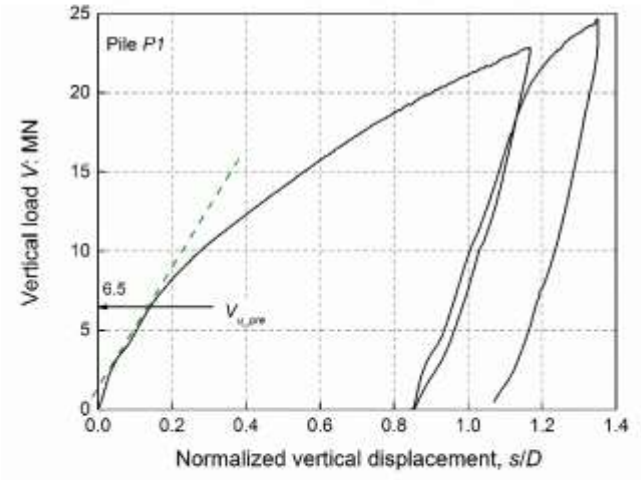

Figure 11 Vertical load-displacement relationship on the pre-installed pile (L/D = 5)

3.3 Influence of vertical loading on *p-y* curves for monopiles

In this section, the impact of vertical loading on the lateral soil reaction-displacement (*p-y*) curves mobilised along the depth of *P1* is discussed.

p-y curves can be derived from bending moment profiles, where *p* is derived by double differentiation of the moment profile, and *y* at discrete locations is obtained by double integration of the moment profile, see Li et al. (2020a) for procedure. The rotation point is assumed at 0.7L along the pile (Fan et al., 2017, Chortis et al., 2020).

Given double differentiation propagates measurement errors it is common to apply curve fitting techniques to minimise these errors, see Xue et al. (2016). Polynomial curve-fitting method (Yang and Liang, 2006) is adopted for curve-fitting the moment data. A 5th order polynomial is used to generate soil reaction (by differentiation) and a 7th order polynomial is used to obtain soil displacements (by integration).

Using this approach, *p*-*y* curves derived from the bending moment profile for test P1-1*g*-L1 (V = 0) are shown in Figure 12. The normalised lateral displacement profiles seen in Figure 12(a) show that the pile lateral displacement (*y*) is almost linearly distributed demonstrating rigid pile behaviour, with 'toe-kick' (Achmus, 2010; Chortis et al. 2020) evident below the rotation point. The corresponding normalised soil reaction profiles along the pile are shown in Figure 12(b) with large resistance mobilised at the pile toe. The data can be combined in the form of *p*-*y* curves in Figure 12(c), which show that the lateral resistance and stiffness increase with depth as expected. It should be noted that the *p*-*y* curve nearest the point of rotation is difficult to extract due to the low lateral displacements experienced by the pile at this location. There is therefore likely some error present with the curve closest this location, in this particular case, the curve at depth 7m. Similar observations have been reported in other literature (Chortis et al. 2020).

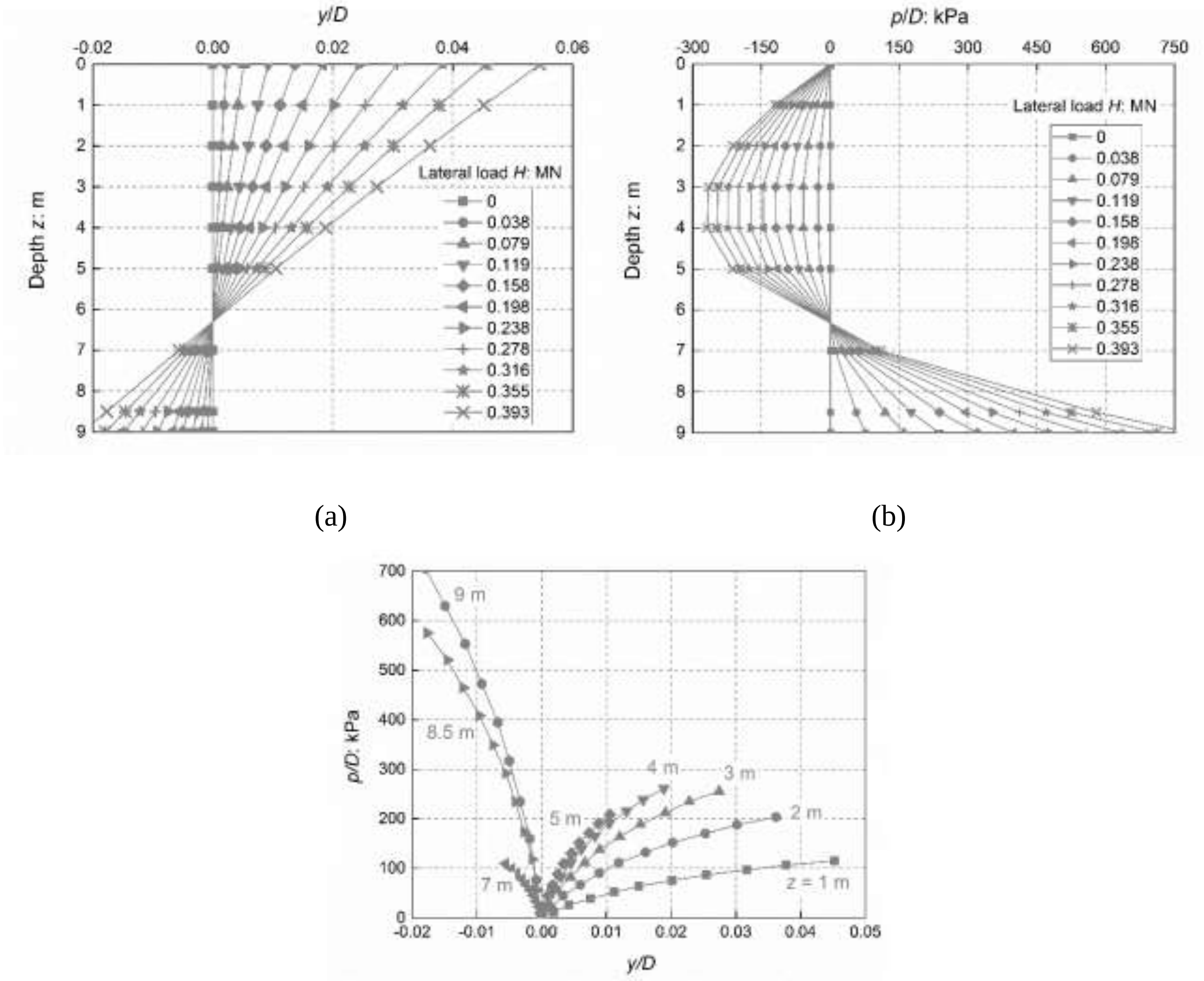

(a) (b)

(c)

Figure 12 Derivation of *p*-*y* curves for test P1-1*g*-L1 (V = 0): (a) Displacement profiles, (b) Soil reaction profiles, and (c) *p*-*y* curves

Figure 13(a-d) show the influence of vertical load level on the normalized derived *p-y* curves at increasing depths, from z = 2 m to 5 m respectively. It is evident that the stiffness and normalised soil reaction (p/D) generally increase as the vertical load level increases from 0 to $0.3V_u$.

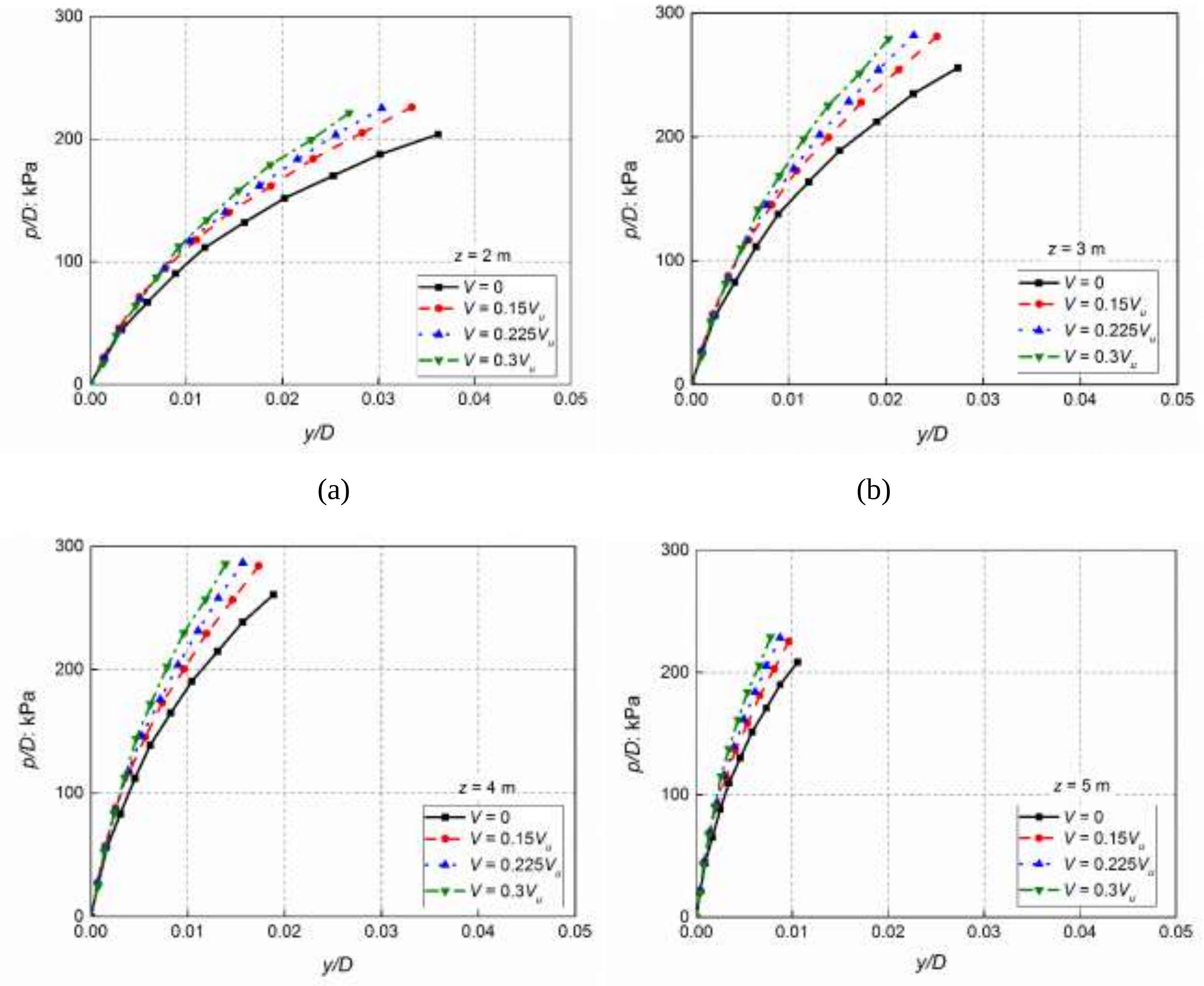

(a) (b)

(c) (d)

Figure 13 Influence of vertical loading on normalized *p-y* curves at various depths (a, b, c, d: z = 2-5 m)

Mu et al. (2018) suggest the influence of applied vertical loading on the soil resistance can be quantified using the following equation:

$$\chi = \frac{p_V - p_0}{p_0} \qquad \text{Equation 2}$$

where χ is the improvement in lateral soil resistance at some reference displacement level due to the application of vertical loading, p_0 is the lateral soil resistance under zero vertical loading and p_V is the lateral soil resistance when the applied vertical load is non-zero. Considering Figure 13(a) (z = 2 m) and taking y/D = 0.01 as the reference displacement level, the normalised soil reaction p_v/D increases by 13%, 16% and 20% over the p_0/D value as the vertical load increases to $0.15V_u$, $0.225V_u$ and $0.3V_u$ respectively. Similar data from all soil depths are summarised in Figure 14, which shows an approximately linear increase of χ as the vertical load level increases. This figure demonstrates the improvement in soil resistance measured under increasing vertical load.

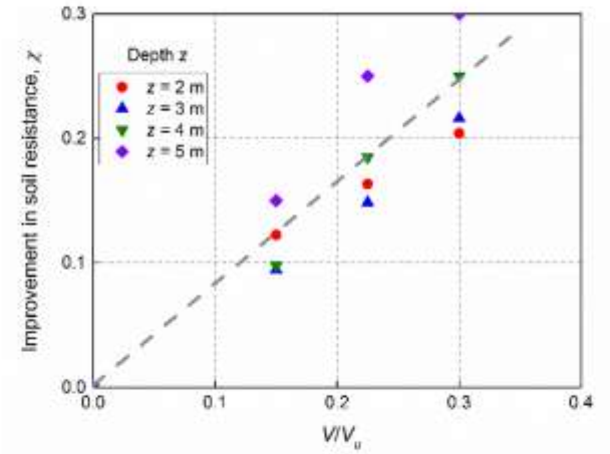

Figure 14 Improvement in soil resistance under applied vertical load (at $y = 0.01D$)

It is of interest to compare the derived *p-y* curves in the present study with those prescribed in offshore design codes, such as the American Petroleum Institute API (2011). The API curves were originally derived from load tests on relatively slender piles. Recognising the limitations for rigid monopiles, several authors have derived *p-y* curves for piles of varying geometries. Choo and Kim (2015) proposed experimental *p-y* curves based on centrifuge tests of 6 m diameter monopiles (at prototype scale) installed in dense sand. Qi et al. (2016) conducted a series of centrifuge tests at a scale of 1:250 to investigate the influence of scour erosion on the lateral behaviour of piles. The model pile used has an equivalent prototype diameter of 2.75 m and an embedded depth of 31.25 m.

The *p-y* curves derived experimentally in this paper were compared with those from API (2011), Choo and Kim (2015), and Qi et al. (2016). To facilitate comparison across scales, p was normalized by $\gamma' D^2$ and y was normalized by D. These curves at a normalized soil depth of $z = 2D$ are shown in Figure 15. The *p-y* curves from this paper correspond well to the *p-y* curve from the pile with L/D = 7.1 from Choo and Kim (2015), which was installed in a single layer of dense sand with D_r = 82-86%. The *p-y* curve derived by Qi et al. (2016) on the other hand exhibits very soft behaviour, though the pile tested has a larger L/D (= 11.4).

For the API *p-y* curves, "failure" is reached at a relatively small lateral displacement (e.g., 0.008*D*). The initial stiffness and strength of the API *p-y* relationship are much greater than those determined from the centrifuge experiments.

The experimental data in Figure 15 suggests that the *p-y* response is very sensitive to *L*/*D*. This is in keeping with the results of major experimental and numerical test programmes such as the recently completed PISA project (Byrne et al., 2019; McAdam et al., 2019). Considering the significant difference between the *p-y* curves determined from the centrifuge experiments and the API recommendations, further large-diameter rigid pile tests should be carried out to formulate the database for establishing design criteria.

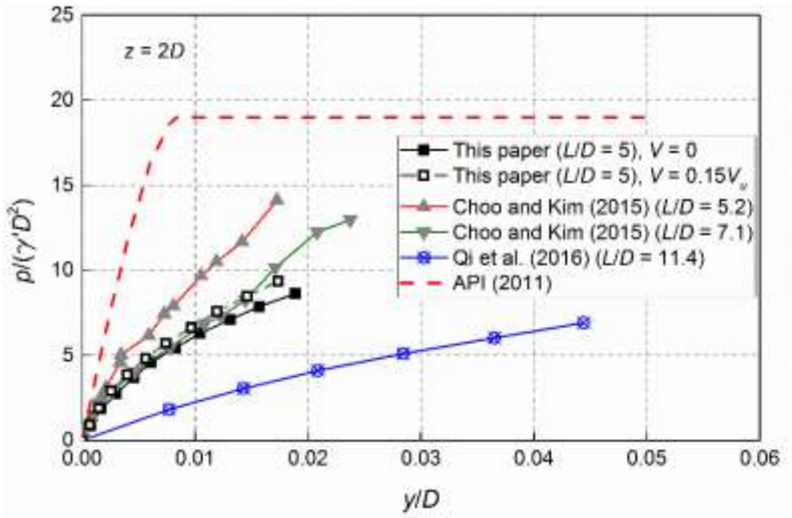

Figure 15 Comparison of normalized *p-y* relationships obtained in this study with those from previous literature at a normalized depth $z = 2D$.

4 Numerical analysis

In this section, the phenomena leading to the observed results in the previous sections are investigated numerically. PLAXIS 3D (Brinkgreve et al., 2015), is used to perform the finite-element (FE) simulations.

4.1 Model

The 3D FE mesh used for the analysis of pile-soil interaction with associated geometrical properties is shown in Figure 16. A model domain width of 20*D*, length of 40*D*, and distance below pile tip of 20*D* was generated, to ensure no boundary effects influenced the results. A comparative model developed with the same boundary distances as the prototype dimensions in the centrifuge tests exhibited only minor effects from boundaries, but this study could not be used to quantify the influence of boundaries due to differences in the chosen stress points between both models. Due to the ease of modelling, the larger model was used in subsequent analyses. Only half the pile section is modelled and a refined mesh is adopted near the pile with a coarser mesh adopted elsewhere. Lateral boundaries are considered smooth and the bottom surface is considered rough. Dry sand was used in the simulations.

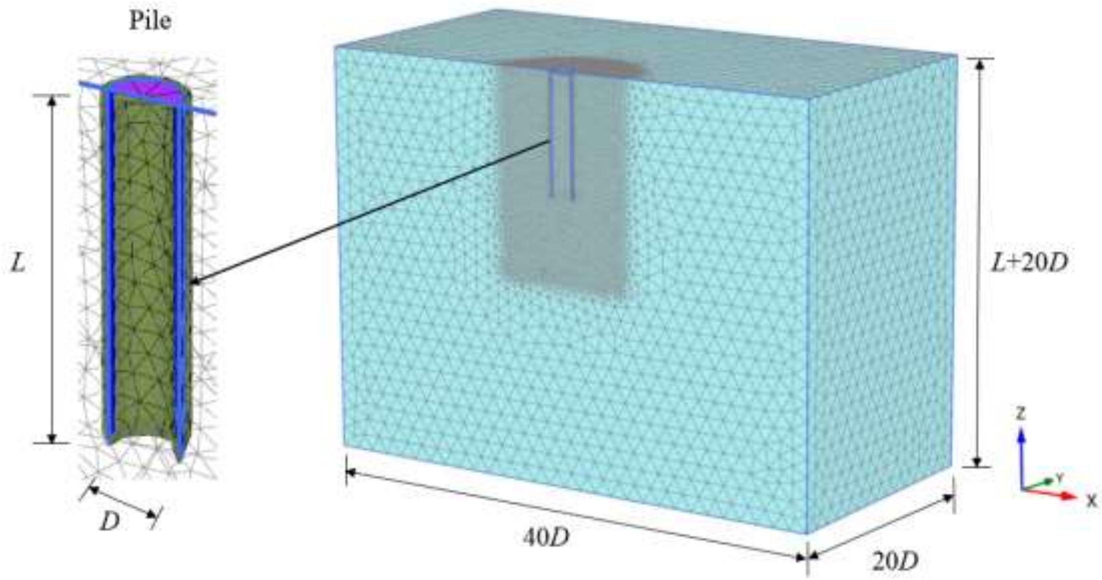

Figure 16 Typical mesh adopted in three-dimensional finite element analysis

Analyses are performed on a single free-headed steel pipe wished-in-place pile in sand. The pile top comprises a rigid plate to enable the application of vertical loads, and the top metre of sand within the pile is removed to prevent interactions occurring. The pile is assumed to be linear elastic with E = 210 GPa and v = 0.3. A Hardening Soil model is used to model the sand, where the parameters are derived based on D_r = 80% (Brinkgreve et al., 2010). Table 4 provides the pile and soil parameters. The relative strength of the interface to the strength of the soil (R_{inter}) is set as 0.7. It should be noted that representative sand parameters are used in the model but it is not intended to model the exact conditions from the experimental tests. Therefore, only qualitative results are sought in this section.

Table 4. Pile geometries and soil properties

No.	Diameter/*D*, m	Embedded length/*L*, m	*L*/*D* ratio	Wall thickness/*t*, mm
1	1.8	5.4	3	30
2	1.8	9	5	30

D_r	γ	E_{50}^{ref}	E_{oed}^{ref}	E_{ur}^{ref}	m	ν_{ur}	φ	ψ	R_f
-	kN/m^3	kN/m^2	kN/m^2	kN/m^2	-	-	o	o	-
80	18.2	48000	48000	144000	0.450	0.2	38	8	0.9

4.2 Change in mean effective stress under vertical loading only

To investigate the mechanism underlying the observed increase in lateral capacity under applied vertical loads, the change in mean effective stress levels around the pile is calculated herein. Under the action of vertical loading only, the change in mean effective stress level measured near the pile in the XZ-plane is shown in Figure 17 for piles with *L/D* of 5 and 3. The change in mean effective stress is obtained by subtracting the mean effective stress profile corresponding to the initial unloaded condition from that corresponding to the applied vertical load of $0.2V_u$, where V_u is obtained by loading the pile in a separate simulation. The mean effective stress level increases substantially in the region surrounding each pile once the vertical loading is applied, suggesting that lateral stiffness and strength will also be increased, offering a potential qualitative explanation of the observed behaviour in the experimental tests.

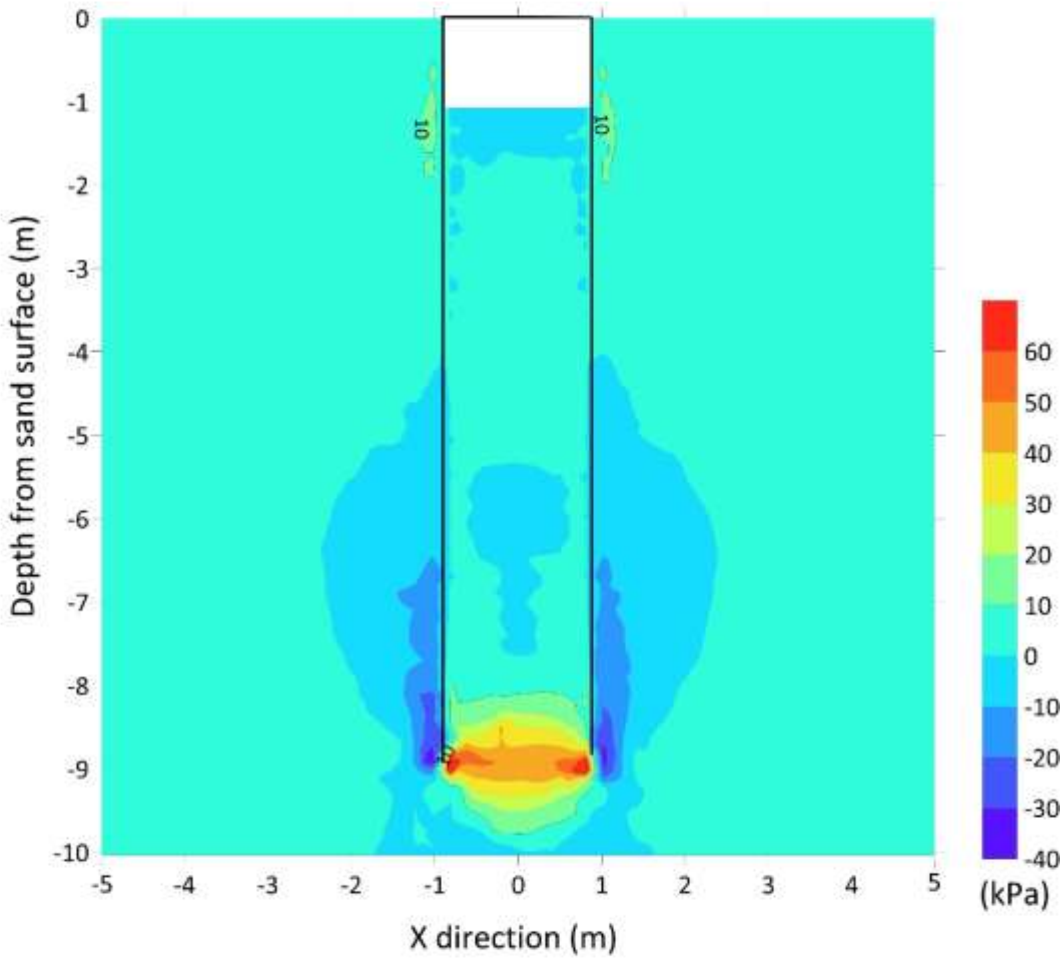

(a)

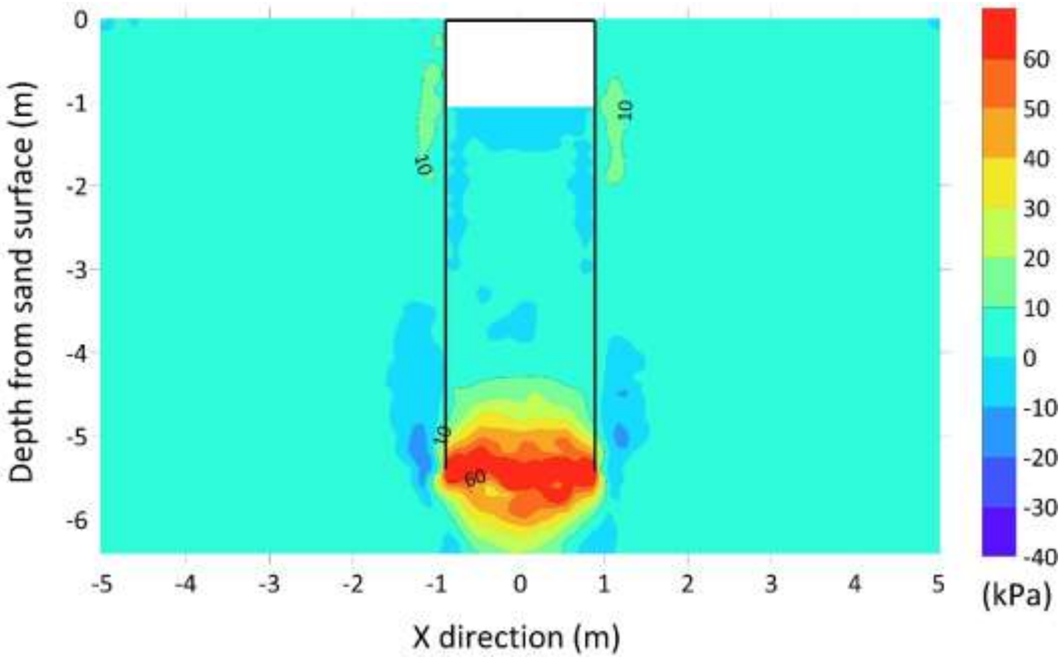

(b)

Figure 17 Change in mean effective stress in the XZ-plane by applying a vertical load of $0.2V_u$: (a) L/D = 5 and (b) L/D = 3

Under the action of vertical loading only, the change in mean effective stress level in the XY-plane is shown in the supplementary material section[1], corresponding to a depth of 1.5D (2.7 m) in the ground. Figure S1(a) shows the data for the pile with L/D = 5, and Figure S1(b) shows that for the pile with L/D = 3. This plot demonstrates the increase in mean effective stress generated around both piles due to the application of vertical loading, and moreover shows that at a given distance from each pile, the increase in mean effective stress on the pile with L/D = 3 is broadly the same as that of the pile with L/D = 5. This is likely a result that the applied vertical loading, $0.2V_u$ is proportional to the ultimate capacity of each pile.

Similar to the evaluation of the influence of applied vertical loading on the soil resistance (Equation 2), the effect of vertical loading on the mean effective stress can be quantified using the following equation:

$$\zeta = \frac{\sigma_{m,V} - \sigma_{m,0}}{\sigma_{m,0}} \qquad \text{Equation 3}$$

[1] See Figure S1

where ζ is defined as the improvement in mean effective stress due to the application of vertical loading, $\sigma_{m,0}$ is the mean effective stress under zero vertical loading, and $\sigma_{m,V}$ is the mean effective stress when the applied vertical load is a non-zero value.

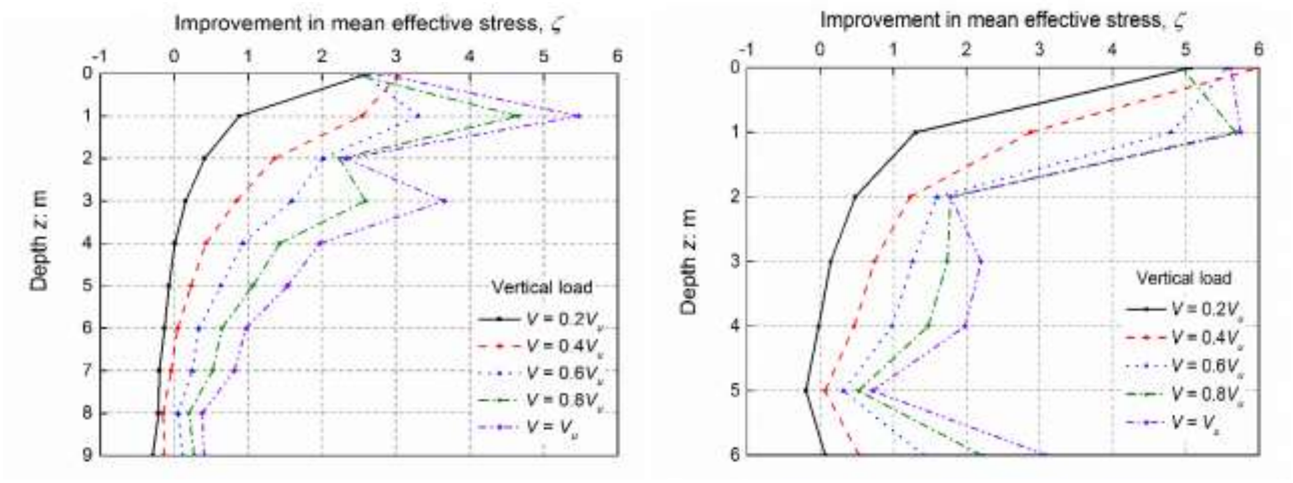

(a) (b)

Figure 18 Improvement in mean effective stress under applied vertical loads along depth of piles: (a) L/D = 5 and (b) L/D = 3

Figure 18(a) and (b) present plots of the improvement in mean effective stress under the influence of vertical loading along the pile embedded length for piles with L/D = 5 and L/D = 3 respectively. Data clearly show that the increase of vertical load increases the mean effective stress at all the soil depths along both piles.

4.3 Change in mean effective stress under vertical loading at a lateral displacement 0.1*D*

At an imposed lateral displacement of 0.1*D* and under the action of vertical loading ($0.2V_u$), the change in mean effective stress measured near the pile in the XZ-plane is shown in Figure 19 for piles with L/D of 5 and 3. The change in mean effective stress is once again obtained by subtracting the mean effective stress profile corresponding to the initial unloaded condition (no V) from that corresponding to the applied vertical load of $0.2V_u$. It should be noted that the loads are applied similar to the load application sequence described in the experimental investigation, namely that vertical loading is applied prior to imposing a lateral displacement. It can be observed that at the imposed lateral displacement (0.1*D*) the mean effective stress level increases substantially in the region surrounding each pile once the vertical loading is applied, which helps to explain the increased pile capacity observed under the action of vertical loading in the experimental investigation (Figure 8).

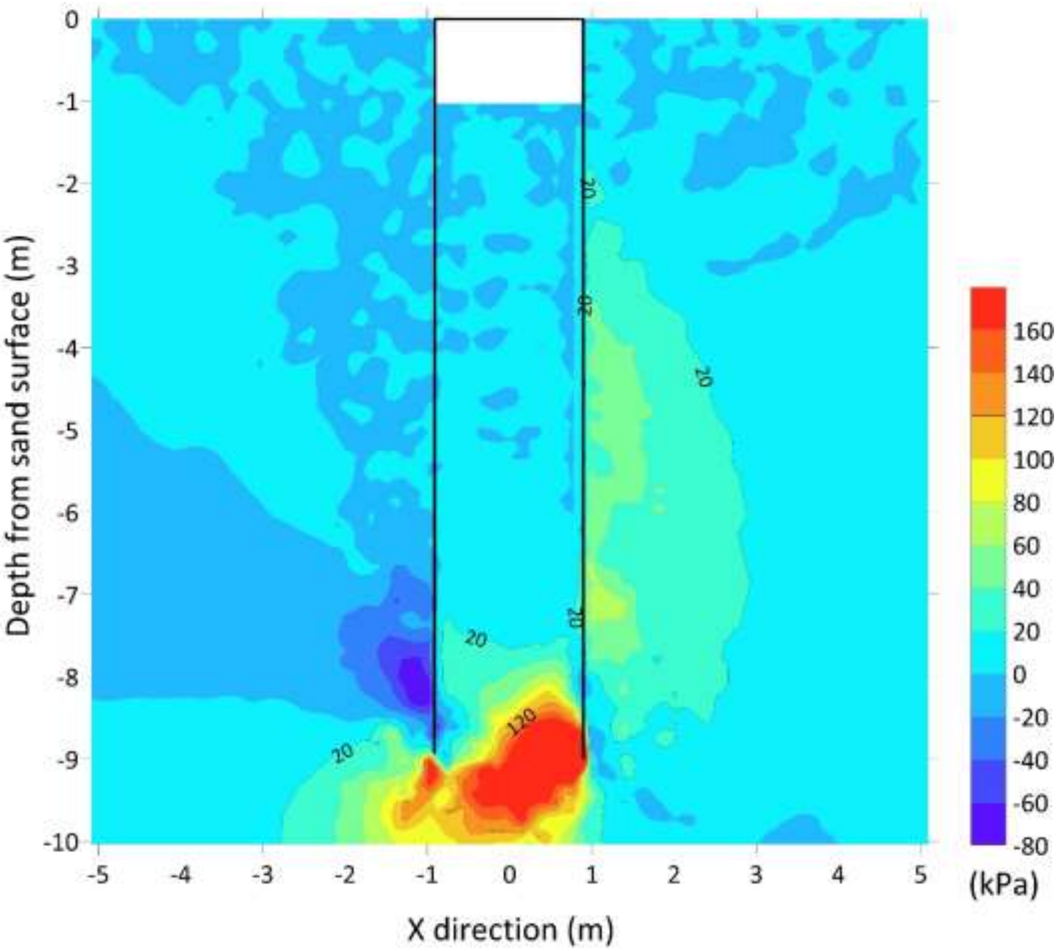

(a)

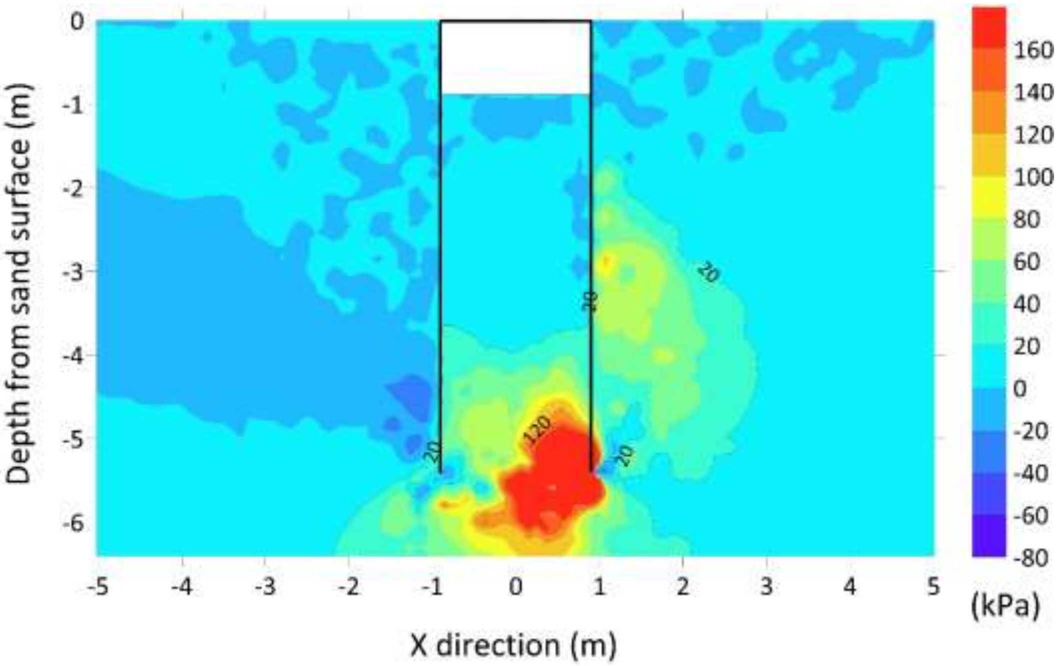

(b)

Figure 19 Change in mean effective stress in the XZ-plane at lateral displacement 0.1*D* by applying a vertical load of $0.2V_u$: (a) L/D = 5 and (b) L/D = 3

The same information as shown in Figure 19 for the pile elevations is also shown in plan view in the supplementary files[2], corresponding to a depth of 1.5D (2.7 m) in the ground. Figure S2(a) shows the data for the pile with L/D = 5, and Figure S2(b) shows that for the pile with L/D = 3. The mean effective stress generated around both piles increases significantly due to the application of vertical loading.

The numerical simulations serve the purpose of qualitatively explaining the mechanism underlying the observed behaviour in the experimental tests conducted in this paper, namely that the increased mean effective stress caused by the application of vertical loading increases the lateral capacity of the piles under subsequent applied lateral loading. The numerical analyses are not intended to explicitly model the conditions in the tests conducted, but to be representative of typical conditions.

5 Conclusions

In this study, an investigation into the influence of vertical loading on the lateral response features of monopiles is conducted using physical (centrifuge) modelling. A series of vertical, lateral and combined load tests were performed on piles installed at 1g and 100g (in-flight) in dry dense sand (D_r = 80%). Numerical simulations were performed to obtain a qualitative understanding of the underlying mechanism on how vertical loading affects pile lateral behaviour. Two different L/D ratios were considered to investigate the effect of pile slenderness. The conclusions drawn from this study can be summarized as follows:

1. The application of vertical loading is beneficial to the lateral load capacity and stiffness of piles with L/D in the range 3 to 5.
2. For piles with an L/D ratio of 5, the beneficial effect of vertical loading increases as the ratio of V/V_u increases.
3. For piles with L/D = 3 the lateral capacity increases initially as the vertical load increases. The normalized pile lateral capacity reaches a peak value when the vertical load is between 0.4V_u and 0.5V_u. For higher vertical loads the beneficial effect of vertical loading reduces.
4. Notwithstanding this the net benefit to the lateral capacity on piles with L/D = 3 is higher than for a pile with L/D = 5 when the ratio V/V_u is below 0.8.
5. For a pile with L/D = 5, the normalised lateral soil resistance p/D measured at a normalised lateral displacement of 0.01D increases approximately linearly as V/V_u increases.

[2] See Figure S2

6. The data show that the method of pile installation has a clear influence on the stiffness and lateral bearing resistance of the piles tested in this study. Installing the piles in-flight leads to a higher retention of lateral effective stress and denser surrounding sand, which manifest as a larger initial stiffness and higher lateral resistance at corresponding displacements than for piles pre-installed at 1*g*.

The test results suggest that the influence of vertical loading on the pile lateral capacity is dependent on the pile L/D ratio. A comparison of the experimental *p*-*y* curves reveals that application of vertical loading increases both the stiffness of the *p*-*y* curves and the soil resistance. An analysis of the influence of pile installation method on resulting *p*-*y* curves was not possible as the instrumented pile could not be installed in-flight due to the potential to damage the instrumentation. The mechanism underlying the observed behaviour is investigated by developing numerical models of both piles (L/D = 5 and 3) using PLAXIS. It is demonstrated that under the action of applying vertical loads, the change in mean effective stress level in the vicinity surrounding each pile is likely responsible for the increased stiffness observed in the experimental tests. Future work will focus on quantifying the benefits obtained under combined loading conditions in a design framework.

Acknowledgements

This work is funded by the Section of Geo-Engineering, Delft University of Technology. The first author received support from the China Scholarship Council (CSC).

References

ACHMUS, M. 2010. *Design of axially and laterally loaded piles for the support of offshore wind energy converters*. Proceedings of the Indian Geotechnical Conference GEOtrendz-2010, Mumbai, India. 92-102.

ALLERSMA, H. 1994. *The University of Delft geotechnical centrifuge*. Centrifuge 94, 47-52.

API, R. 2011. 2GEO (2011) *Geotechnical and foundation design considerations*. American Petroleum Institute, Washington, DC, USA.

BRANSBY, M. & RANDOLPH, M. 1998. *The effect of skirted foundation shape on response to combined V-MH loadings*. The Eighth International Offshore and Polar Engineering Conference. International Society of Offshore and Polar Engineers.

BRINKGREVE, R., ENGIN, E. & ENGIN, H. 2010. *Validation of empirical formulas to derive model parameters for sands.* Numerical methods in geotechnical engineering. 137-42.

BRINKGREVE, R., KUMARSWAMY, S. & SWOLFS, W. 2015. *Plaxis 3D Anniversary Edition Manual*. Plaxis bv, Delft, The Netherlands, Delft.

BUTTERFIELD, R. & GOTTARDI, G. 1994. *A complete three-dimensional failure envelope for shallow footings on sand*. Géotechnique, 44(1), 181-184.

BYRNE, B. W., BURD, H. J., ZDRAVKOVIĆ, L., MCADAM, R. A., TABORDA, D. M., HOULSBY, G. T., JARDINE, R. J., MARTIN, C. M., POTTS, D. M. & GAVIN, K. G. 2019. *PISA: new design methods for offshore wind turbine monopiles.* Revue Française de Géotechnique, 158, 3.

CHOO, Y. W. & KIM, D. 2015. *Experimental Development of the p-y Relationship for Large-Diameter Offshore Monopiles in Sands: Centrifuge Tests.* Journal of Geotechnical and Geoenvironmental Engineering, 142(1), 04015058.

CHORTIS, G., ASKARINEJAD, A., PRENDERGAST, L., LI, Q. & GAVIN, K. 2020. *Influence of scour depth and type on p-y curves for monopiles in sand under monotonic lateral loading in a geotechnical centrifuge.* Ocean Engineering, 106838.

DE JAGER, R. R., MAGHSOUDLOO, A., ASKARINEJAD, A. & MOLENKAMP, F. 2017. *Preliminary results of instrumented laboratory flow slides.* 1st International Conference on the Material Point Method. Delft, The Netherlands: Elsevier Ltd.

De NICOLA, A. 1996. *The Performance of Pipe Piles in Sand*. Doctoral dissertation, University of Western Australia, Perth, Australia.

De NICOLA, A. & RANDOLPH, M.F. 1997. *The plugging behaviour of driven and jacked piles in sand*. Géotechnique 47(4), 841–856.

DYSON, G.J. & RANDOLPH, M.F. 2001. *Monotonic lateral loading of piles in calcareous sand*. Journal of Geotechnical and Geoenvironmental Engineering, 127(4), 346-352.

FAN, S., BIENEN, B. & RANDOLPH, M. F. 2019. *Centrifuge study on effect of installation method on lateral response of monopiles in sand.* International Journal of Physical Modelling in Geotechnics, 1-13.

GARNIER, J., GAUDIN, C., SPRINGMAN, S. M., CULLIGAN, P., GOODINGS, D., KONIG, D., KUTTER, B., PHILLIPS, R., RANDOLPH, M. & THOREL, L. 2007. *Catalogue of scaling laws and similitude questions in geotechnical centrifuge modelling*. International Journal of Physical Modelling in Geotechnics, 7(3), 1-23.

HTC-SENSOR TAL220. http://www.htc-sensor.com/products/162.html

ISO 19901-4, *Petroleum and natural gas industries-Specific requirements for offshore structures-Part 4: Geotechnical and foundation design considerations*

JAIN, N., RANJAN, G. & RAMASAMY, G. 1987. *Effect of vertical load on flexural behaviour of piles.* Geotechnical Engineering, 18, 2.

KARASEV, O., TALANOV, G. & BENDA, S. 1977. *Investigation of the work of single situ-cast piles under different load combinations.* Soil Mechanics and Foundation Engineering, 14(3), 173-177.

KARTHIGEYAN, S., RAMAKRISHNA, V. & RAJAGOPAL, K. 2007. *Numerical investigation of the effect of vertical load on the lateral response of piles.* Journal of Geotechnical and Geoenvironmental Engineering, 133(5), 512-521.

KLINKVORT, R. & HEDEDAL, O. 2010 *Centrifuge modelling of offshore monopile foundation.* In Frontiers in offshore Geotechnics II: Proceedings of the 2nd International Symposium Frontiers in Offshore Geotechnics (ISFOG2010) (Gourvenec SM and White D (eds)). Taylor and Francis, London, UK, 581-586.

LEE, J. 2008. *Experimental investigation of the load response of model pilesin sand.* PhD thesis. Purdue University.

Li, Q. , ASKARINEJAD, A. & GAVIN, K. 2020a. *The impact of scour on the lateral resistance of wind turbine monopiles: an experimental study*. Canadian Geotechnical Journal.

LI, Q. , ASKARINEJAD, A. & GAVIN, K. 2020b. *Lateral response of rigid monopiles subjected to cyclic loading: centrifuge modelling*. Proceedings of the Institution of Civil Engineers - Geotechnical Engineering.

LI, Q., PRENDERGAST, L., ASKARINEJAD, A. & GAVIN, K. 2018. *Effect of scour on the behavior of a combined loaded monopile in sand.* 9th European Conference on Numerical Methods in Geotechnical Engineering, Porto, Portugal.

LI, Q., PRENDERGAST, L., ASKARINEJAD, A., & GAVIN, K. 2020c. *Influence of vertical loading on behavior of laterally-loaded foundation piles: a review*. Journal of Marine Science and Engineering, 8(12) 1029

LI, Q., PRENDERGAST, L., ASKARINEJAD, A., CHORTIS, G. & GAVIN, K. 2020d. *Centrifuge Modeling of the Impact of Local and Global Scour Erosion on the Monotonic Lateral Response of a Monopile in Sand.* Geotechnical Testing Journal, 43, 5.

LU, W. & ZHANG, G. 2018. *Influence mechanism of vertical-horizontal combined loads on the response of a single pile in sand*. Soils and foundations, 58(5), 1228-1239.

MAGHSOUDLOO, A., ASKARINEJAD, A., DE JAGER, R., MOLENKAMP, F. & HICKS, M. 2018. *Experimental investigation of pore pressure and acceleration development in static liquefaction induced failures in submerged slopes.* Physical Modelling in Geotechnics, Volume 2. CRC Press.

MCADAM, R. A., BYRNE, B. W., HOULSBY, G. T., BEUCKELAERS, W. J., BURD, H. J., GAVIN, K. G., IGOE, D. J., JARDINE, R. J., MARTIN, C. M. & MUIR WOOD, A. 2019. *Monotonic laterally loaded pile testing in a dense marine sand at Dunkirk.* Géotechnique, 1-13.

MU, L., KANG, X., FENG, K., HUANG, M. & CAO, J. 2018. *Influence of vertical loads on lateral behaviour of monopiles in sand.* European Journal of Environmental and Civil Engineering, 22, sup1, 286-301.

MURPHY, G., IGOE, D., DOHERTY, P., and GAVIN, K. 2018. *3D FEM Approach for Laterally Loaded Monopile Design*. Computersand Geotechnics, 100, 76–83.

NOVA, R. & MONTRASIO, L. 1991. *Settlements of shallow foundations on sand.* Géotechnique, 41(2), 243-256.

NUNEZ, I., HOADLEY, P., RANDOLPH, M. & HULETT, J. 1988. *Driving and tension loading of piles in sand on a centrifuge.* Centrifuge, 353-362.

PRAKASHA, K., JOER, H. & RANDOLPH, M. 2005. *Establishing a model testing capability for deep water foundation systems.* Proceedings of the 15th International Offshore and Polar Engineering Conference and Exhibition. Korea, Seoul. 309-315.

QI, W., GAO, F., RANDOLPH, M. & LEHANE, B. 2016. *Scour effects on p-y curves for shallowly embedded piles in sand.* Géotechnique, 66(8), 648-660.

SIMBATOUCH SBT620. https://www.china.cn/chengzhongchuanganqi/4378290334.html

WINDEUROPE 2018. 2018. *Offshore Wind in Europe: Key trends and statistics 2017.*

XUE, J., GAVIN, K., MURPHY, G., DOHERTY, P. & IGOE, D. 2016. *Optimization technique to determine the py curves of laterally loaded stiff piles in dense sand.* Geotechnical Testing Journal, 39(5), 842-854.

YANG, K. & LIANG, R. 2006. *Methods for deriving py curves from instrumented lateral load tests.* Geotechnical testing journal, 30(1), 31-38.

ZHANG, W. & ASKARINEJAD, A. 2019a. *Behaviour of buried pipes in unstable sandy slopes.* Landslides, 16(2), 283-293.

ZHANG, W. & ASKARINEJAD, A. 2019b. *Centrifuge modelling of submarine landslides due to static liquefaction.* Landslides 16(10), 1921-38.